Functional organization of sensory input to the olfactory bulb glomerulus analyzed by two-photon calcium imaging

Matt Wachowiak*, Winfried Denk†, and Rainer W. Friedrich†‡

*Department of Biology, Boston University, 5 Cummington Street, Boston, MA 02215; and †Department of Biomedical Optics, Max Planck Institute for Medical Research, Jahnstrasse 29, D-69120 Heidelberg, Germany

Edited by Charles F. Stevens, The Salk Institute for Biological Studies, La Jolla, CA, and approved May 10, 2004 (received for review January 20, 2004)

Glomeruli in the olfactory bulb are anatomically discrete modules receiving input from idiotypic olfactory sensory neurons. To examine the functional organization of sensory inputs to individual glomeruli, we loaded olfactory sensory neurons with a Ca^{2+} indicator and measured odorant-evoked presynaptic Ca^{2+} signals within single glomeruli by using two-photon microscopy in anaesthetized mice. Odorants evoked patterns of discrete Ca^{2+} signals throughout the neuropil of a glomerulus. Across glomeruli, Ca^{2+} signals occurred with equal probability in all glomerular regions. Within single glomeruli, the pattern of intraglomerular Ca^{2+} signals was indistinguishable for stimuli of different duration, identity, and concentration. Moreover, the response time course of the signals was similar throughout the glomerulus. Hence, sensory inputs to individual glomeruli are spatially heterogeneous but seem to be functionally indiscriminate. These results support the view of olfactory glomeruli as functional units in representing sensory information.

Odorants are first detected in the mammalian nose by olfactory sensory neurons (OSNs), each of which sends an unbranched axon to one of the ≈2,000 glomeruli of the olfactory bulb (OB), where it makes approximately eight synaptic connections with local interneurons and the principal output neurons of the OB (mitral/tufted cells) (1–3). Glomeruli consist of a dense neuropil enclosed by glial cells and are among the most distinctive anatomical modules in the brain, giving rise to the hypothesis that they function as units in olfactory information processing (4–7). Because odorants stimulate odorant- and concentration-specific ensembles of glomeruli (8–14), odor information is thought to be encoded by combinatorial patterns of glomerular activity (6, 15, 16).

Glomeruli have long been considered functional units in coding olfactory information (3, 5–8). Most or all of the ≈12,000 OSNs (3) converging onto a glomerulus express the same single odorant receptor from a repertoire of ≈1,000 genes (17–21). Furthermore, odorant-evoked 2-deoxyglucose uptake seems to be nearly uniform within glomeruli (8). A glomerulus may therefore be innervated by OSNs responding similarly to odorants and, indeed, constitute a functional unit. Other results, however, raise the possibility that sensory input to a glomerulus is not functionally homogeneous. First, convergent OSNs are dispersed across broad zones of the olfactory epithelium (22) and may be exposed to different odorant concentrations and time courses during odor sampling *in vivo*. Consequently, the magnitude and time course of OSN odorant responses varies across the nasal epithelium (23–25). Second, dissociated OSNs expressing the same odorant receptor have similar odorant response profiles but not always similar sensitivities (26). Third, response properties of idiotypic OSNs may be diversified by modulatory processes acting in the nasal epithelium (27, 28) or at the axon terminals in the glomerulus (29–31). Finally, the synaptic organization within a glomerulus is heterogeneous. OSN axons and dendrites of OB neurons are segregated into interdigitating compartments (32–35). In some glomeruli, subpopulations of OSNs distinguished by histochemical markers terminate in discrete subregions of the axonal compartment (36, 37). These data raise the possibility that functionally distinct subdivisions exist within a glomerulus.

Direct measurements of the activity of glomerular afferents have been difficult because most functional measures of intraglomerular activity lack sufficient spatial resolution or cellular specificity. Here, we loaded OSNs with a fluorescent Ca^{2+} indicator and measured patterns of afferent presynaptic activity within glomeruli by two-photon Ca^{2+} imaging in anaesthetized mice. Our data indicate that OSN input to individual glomeruli is spatially heterogeneous but functionally homogeneous at the resolution of our two-photon measurements. Hence, glomerular inputs show similar odorant response properties *in vivo*, supporting the hypothesis that the glomerulus represents a functional unit that integrates sensory input from a large population of idiotypic OSNs.

Methods

Dye Loading and Preparation. OSNs were loaded *in vivo* with calcium green-1 dextran or Oregon green 488 BAPTA-1 dextran (10 kDa; Molecular Probes) in 8- to 12-wk-old C57/Bl6 mice as described in ref. 12. Experiments were performed 4–8 days after loading on freely breathing and artificially sniffing mice anaesthetized with pentobarbital (50 mg/kg, i.p.) as described in ref. 12.

A custom microscope allowed for wide-field or two-photon imaging through the same objective (X20, 0.95 numerical aperture water immersion; Olympus, Melville, NY). Wide-field illumination used a 150-W Xenon arc lamp attenuated to 1.5–25% of full intensity and filters 495/30 (exciter), 520LP (dichroic), and 545/50 (emitter). The epifluorescence condensor was coupled to a custom-built microscope head containing the tube lens, mirrors, and stepper motors to move the objective in three dimensions while keeping the optical path nearly constant. The emitted light was projected onto the chip (1,040 × 1,392 pixels) of a CCD camera (CoolSnapHQ, Photometrics, Tucson, AZ). Images were binned 4 × 4 or 8 × 8 and digitized at 12 bits and 10–45 Hz.

Two-photon fluorescence was excited by a mode-locked Ti:Sapphire laser (Mira900, 100 fs, 76 MHz; pumped by a 10-W Verdi laser; 930 nm; Coherent, Santa Clara, CA). A dichroic mirror (789 DCSPR) was inserted close to the back aperture of the objective to reflect emitted light through external detection optics and an emission filter (515/30) onto a photomultiplier tube (Hamamatsu R6357). Image acquisition was controlled by custom software (CFNT, written by R. Stepnoski of Bell Labs and

This paper was submitted directly (Track II) to the PNAS office.

Abbreviations: OSN, olfactory sensory neuron; OB, olfactory bulb.

‡To whom correspondence should be addressed. E-mail: rainer.friedrich@mpimf-heidelberg.mpg.de.

M. Müller of the Max Planck Institute for Medical Research). Images of the resting fluorescence in individual glomeruli had 256 × 256 pixels or 128 × 128 pixels. Odorant-evoked Ca^{2+} signals were usually recorded at 64 × 64 pixel resolution and 8 Hz. For faster measurements, scans of 8 × 64 pixels or 1 × 64 pixels were acquired at 62.5 or 500 Hz, respectively. Laser intensity was adjusted to minimize photobleaching.

Odorant Stimulation. The saturated vapor of odorants (95–99% pure) in reservoirs of a flow dilution olfactometer (38) was diluted with ultrapure air by using mass flow controllers (Pneucleus, Hollis, NH), generating a constant flow rate of 0.5–1 liters/min. The design minimized cross-contamination and allowed for precise control of stimulus timing and concentration. Artificially sniffing mice were double-tracheotomized to control odorant access to the nasal cavity independent of respiration (11). The contralateral naris was plugged and square pulses of negative pressure (60–75 ml/min flow rate, 150-ms duration, 3.3 Hz) were applied to the upper tracheotomy tube (12). Nasal patency in each sniff was monitored with a pressure sensor (Sigmann Elektronik, Hüffenhardt, Germany). Sniffing was maintained throughout the experiment, with brief rest periods every several minutes. Cleaned, humidified air was continuously blown over the nares to prevent drying and switched off during odorant presentation.

Stimulus durations were 2–3 s and separated by a minimum of 45 s. Data acquisition was triggered on the artificial sniff cycle. Presentations of different stimuli were typically interleaved.

Data Analysis. Odorant-evoked signals were easily detected in single trials (Fig. 1*C*) and stable for hours in wide-field and two-photon modes. All individual trials were inspected for consistency of overall response amplitude. Datasets showing drift of the optical section over trials were excluded from the analysis. Data from 10 freely breathing and 15 artificially sniffing mice were analyzed. Data from another 23 mice were used to optimize the imaging procedure but excluded from quantitative analysis because experimental conditions varied across experiments.

Data processing and display was performed with custom software written in IGORPRO (WaveMetrics, Lake Oswego, OR) and MATLAB (MathWorks, Natick, MA). For two-photon data, time series of raw images from 4–16 presentations of the same odorant were averaged to improve the signal-to-noise ratio. A baseline frame averaged over 9–17 frames (constant for each experiment) before odor application was used to generate time series of frames showing the relative change in fluorescence in each pixel ($\Delta F/F$ series). Maps of evoked Ca^{2+} signals were constructed by averaging successive $\Delta F/F$ frames during odorant presentation (usually eight frames, corresponding to 1 s) and low-pass spatially filtered with a Gaussian kernel of $\sigma = 1.2$ pixels (width of 5 pixels) to further reduce shot noise. No temporal filter was applied.

Activity maps in cross sections through individual glomeruli consisted of 64 × 64 pixels covering an area of ≈80 × 80 μm, varying slightly with glomerular size. This pixel resolution was chosen to optimize three critical parameters: spatial resolution, imaging speed, and signal-to-noise ratio. After low-pass spatial filtering of the response maps, signals from structures ≥4 pixels (≈5 μm) apart could be resolved as distinct from each other, by the conventional criterion that the signal overlap of equally strong signals is ≤50%. However, differences in the maps of odorant-evoked signals were still measurable with a resolution ultimately limited by the pixel resolution of the image (≈1.2 μm per pixel).

Quantitative comparison of activity maps was restricted to data obtained under artificial sniffing. All activity maps for quantitative comparisons were constructed from averages over four trials and eight $\Delta F/F$ frames covering the peak of the odor response (except for comparisons of different time windows). Glomerular borders were outlined manually, and pixels outside the glomerulus were excluded from analysis. The same outline was applied to all maps from the same optical section. The Pearson correlation coefficient was used to quantify the similarity of signal maps because it depends on the relative distribution of $\Delta F/F$ values in the pattern and is independent of absolute response intensity. Alternatively, activity maps were normalized to their mean values, subtracted from each other, and the mean absolute difference between maps was taken as a measure of similarity. This measure is related to the correlation but does not use squared difference values.

For calculation of signal-to-noise ratio, noise was measured as the rms $\Delta F/F$ signal before stimulus onset. The noise map was generated from eight $\Delta F/F$ frames, with the baseline (F) derived from the previous eight frames. The signal was determined as the average of the 20 highest pixel values in the $\Delta F/F$ map evoked

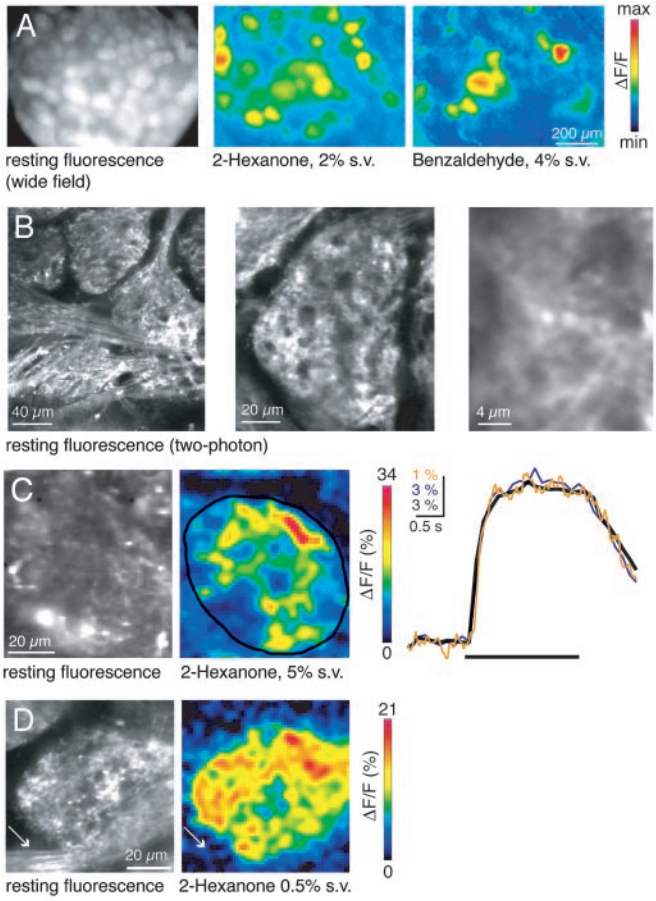

Fig. 1. Two-photon imaging reveals patterns of intraglomerular presynaptic Ca^{2+} signals. (*A*) Wide-field fluorescence imaging of glomeruli after loading of OSN axons with calcium green-1 dextran (*Left*) and activity patterns evoked by two odorants (*Center* and *Right*). Imaging was performed *in vivo* through the thinned skull in a freely breathing animal. Color scale: −1.75 to 7% for 2-hexanone, and −1 to 4% for benzaldehyde. (*B*) *In vivo* two-photon scans of different glomeruli at increasing magnification after loading of OSN axons with calcium green-1 dextran or Oregon green BAPTA-1 dextran. (*C*) Two-photon imaging of resting fluorescence and intraglomerular Ca^{2+} signals in an optical section through an individual glomerulus. (*Right*) Response time course in the outlined region. Yellow, wide-field imaging, single trial; blue, two-photon imaging, single trial; black, two-photon imaging, average of eight trials. (*D*) Odorant-evoked Ca^{2+} signals in an optical section through a glomerulus and innervating axon bundle (arrow).

by the subsequent odor stimulation. The quotient of these values is a conservative estimate of the signal-to-noise ratio. The noise in the activity maps used for the comparison analysis was usually lower because the baseline was averaged over more than eight frames.

For measurements of hot spot diameter, a strongly smoothed image (Gaussian filter with $\sigma = 115$ pixels) was subtracted from the activity map to enhance hot spot contrast. The diameter of isolated hot spots was measured along the longest axis.

Results

Two-Photon Ca^{2+} Imaging of Intraglomerular Activity Patterns. Individual glomeruli of the dorsal OB could be clearly distinguished through the thinned skull by wide-field microscopy with a X20 objective (numerical aperture 0.95) after loading OSNs with calcium green-1 dextran or Oregon green 488 BAPTA-1 dextran. Odorants evoked fluorescence changes in subsets of these glomeruli, reflecting odorant-specific patterns of OSN input across the glomerular array (Fig. 1*A*) (12, 13). However, light scattering and out-of-focus light precluded the resolution of structures in single glomeruli *in vivo*. As a result, the wide-field fluorescence signal within a glomerulus seemed homogeneous.

By using two-photon microscopy, structural details within single glomeruli could be easily resolved. Glomeruli were often innervated by multiple axon fascicles and contained volumes devoid of labeled afferents (Fig. 1*B*) (34, 35), confirming that the Ca^{2+} indicator was confined to OSN axons (10, 12, 13). At higher magnification, a complex pattern of axon fascicles and boutons was observed within the glomerular neuropil (Fig. 1*B Right*).

Odorants evoked fluorescence changes with a time course similar to that measured with wide-field optics in the same glomerulus (Fig. 1*C*). The magnitude of the relative fluorescence change was greater in the two-photon than in the wide-field mode, presumably because light from nonresponding axons in the olfactory nerve layer was excluded. In single trials, however, the signal-to-noise ratio was often lower due to shot noise resulting from the smaller number of measured photons. This is an inevitable consequence of the increased spatial resolution because the total number of photons that can be generated in a thin optical section without excessive photodamage is limited.

Size and Distribution of Ca^{2+} Signals. The spatial distribution of Ca^{2+} signals in optical sections through a glomerulus was heterogeneous and comprised multiple foci, or "hot spots" (Fig. 1*C*). Small or no Ca^{2+} signals were observed in extraglomerular axon fascicles close to the glomerular neuropil (Fig. 1*D*), confirming that Ca^{2+} entry along projecting axons was negligible (10, 12, 13). At high magnification, the discrete nature of the hot spots was clearly apparent (Fig. 2 *A* and *B*). Thus, odorant-evoked Ca^{2+} signals occurred only in distal compartments of OSN axons and were highly localized, consistent with the interpretation that they arise from Ca^{2+} influx into presynaptic terminals.

The mean diameter of the Ca^{2+} signal hot spots, measured from Ca^{2+} signal maps at high spatial resolution (<0.5 μm per pixel) after contrast enhancement (see *Methods*), was 1.8 ± 0.7 μm (mean $\pm$ SD; $n = 304$), implying that hot spots represent the activation of a small number of terminals. At high temporal resolution, rapid fluctuations of the Ca^{2+} signal in individual hot spots were observed (Fig. 2*C*) that were variable from trial to trial, consistent with the conclusion that a small number of Ca^{2+} sources underlies each hot spot. Fluctuations in adjacent hot spots were uncorrelated, suggesting that most hot spots contain terminals of different OSNs.

Hot spots were distributed throughout the glomerular volume (Fig. 2*D*), as revealed by maps of Ca^{2+} signals evoked by the same odorant at different focal planes (2–10 planes in each of 14 glomeruli). To determine whether OSN inputs are distributed

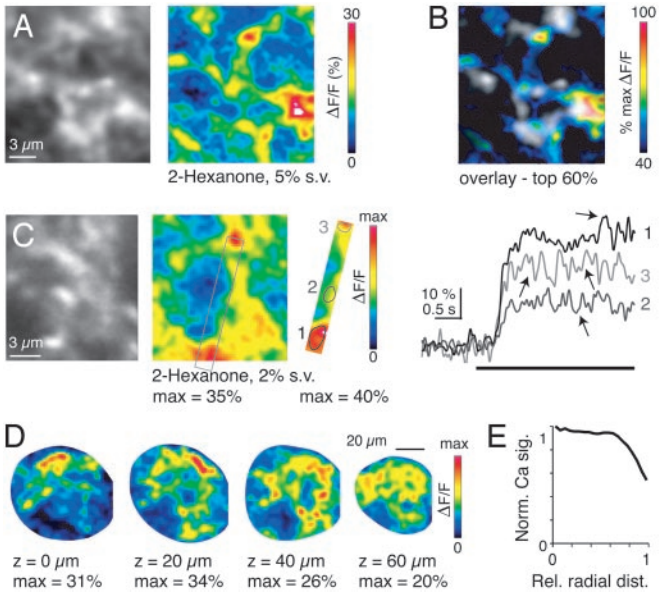

Fig. 2. Distribution of odorant-evoked intraglomerular Ca^{2+} signals. (*A*) High spatial resolution image of fluorescence within the glomerular neuropil (*Left*) and map of odorant-evoked Ca^{2+} signal in the same region (*Right*). (*B*) Overlay of resting fluorescence and odorant-evoked Ca^{2+} signal map in *A*, rescaled and thresholded at 40% of their maxima. (*C*) Temporal structure of Ca^{2+} signals. Resting fluorescence (*Left*) and odorant-evoked Ca^{2+} signals (*Center*) within a glomerulus (high magnification). The area approximated by the gray rectangle was subsequently scanned at high temporal resolution (frame rate, 62.5 Hz). (*Right*) Time courses were smoothed by a running average over three adjacent data points. Arrows depict uncorrelated signal fluctuations. (*D*) Maps of Ca^{2+} signals evoked by 2-hexanone (5%) at different depths in the same glomerulus. $Z = 0$ μm corresponds to a level just below the olfactory nerve layer. White mask outlines glomerular border. (*E*) Normalized average intraglomerular Ca^{2+} signal as a function of radial position in the glomerular cross section.

preferentially in particular subglomerular regions, we analyzed the average radial distribution of Ca^{2+} signals within glomeruli. The Ca^{2+} signal as a function of the relative radial distance from the center of an optical section was averaged over sections and normalized to the maximum. The resulting distribution revealed no preferential radial domain of OSN input (Fig. 2*E*). Rather, Ca^{2+} signals occurred, on average, with equal probability through most of the glomerular cross section and fell off only at the perimeter.

Odor Dependence of Intraglomerular Activity Patterns. If sensory inputs to a glomerulus are functionally similar, then intraglomerular patterns of Ca^{2+} signal hot spots evoked by different stimuli should be indistinguishable. We measured Ca^{2+} signal patterns in optical sections of $\approx 80 \times 80$ μm through a single glomerulus, scanned with a pixel resolution of 64×64 at a frame rate of 8 Hz. The resulting spatial resolution (≈ 1.2 μm per pixel) approaches the spatial resolution limit of two-photon microscopy [0.5–1 μm laterally and 2–3 μm in depth (39)]. For each stimulus, four repeated trials were averaged by using an artificial sniff paradigm that preserved sniff timing across trials. Response maps were constructed from 1-s time windows and slightly smoothed, thereby reducing the spatial resolution to ≈ 5 μm (see *Methods*) but increasing the signal-to-noise ratio. The average signal-to-noise ratio in these intraglomerular activity maps was 12 ± 4 (mean $\pm$ SD; range, 6–20).

Intraglomerular activity maps evoked by repeated applications of the same odorant were similar but showed some variability (Fig. 3*A*). This variability may arise from shot noise,

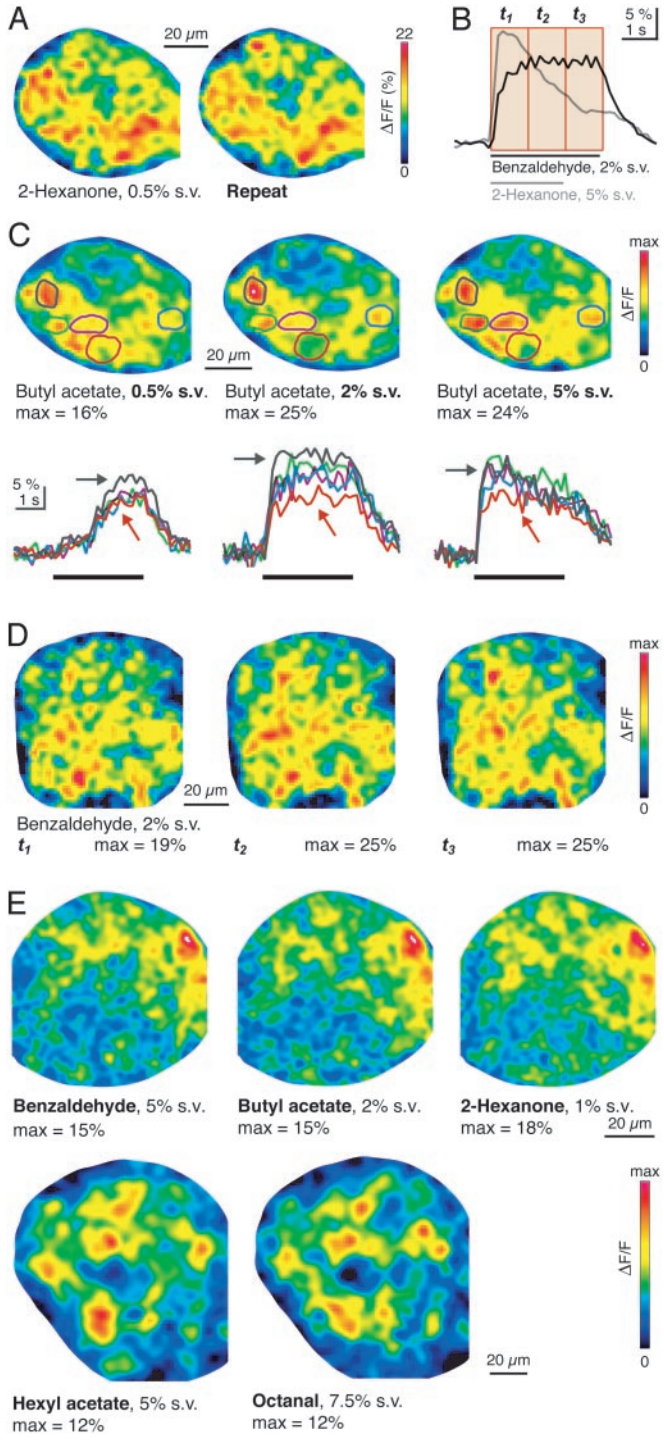

Fig. 3. Stimulus dependence of odorant-evoked maps of intraglomerular Ca^{2+} signals. (*A*) Intraglomerular patterns of Ca^{2+} signals evoked by repeated stimulation with the same odorant. White mask outlines glomerular border. (*B*) Time course of the response of the glomerulus in *D*, averaged over the entire cross section. Red boxes depict the time windows used to construct the activity maps in *D*. Gray trace shows the response to a different odorant (2-hexanone, 5%), which evoked a different temporal response. (*C*) Intraglomerular activity maps evoked by increasing concentrations of the same odorant. Traces show time courses of the Ca^{2+} signal in the regions outlined by corresponding line colors. (*D*) Maps evoked by benzaldehyde (2%) in subsequent 1-s time windows during a 3-s odorant presentation. The response time course is shown in *B*. (*E*) Intraglomerular activity maps evoked by three different odorants in one glomerulus (*Upper*) and two different odorants in another glomerulus (*Lower*).

small ongoing movement in the intact brain (caused, e.g., by heartbeat), and trial-to-trial response variability. The similarity of activity maps evoked by repeated applications of the same odorant was quantified by the Pearson correlation. The average correlation coefficient was 0.69 ± 0.13 ($n = 47$).

The time course of the Ca^{2+} signal, spatially averaged over the glomerular cross section, could vary substantially with odorant identity and concentration (Fig. 3 *B* and *C*). For example, Fig. 3*B* shows the time course of responses to the odorants benzaldehyde and 2-hexanone. The response to benzaldehyde increased during the first second of the response and then reached a plateau. This plateau does not reflect saturation of the Ca^{2+} indicator, because 2-hexanone evoked a larger signal in the same location. For a given stimulus, however, the response time course was similar throughout the glomerulus (Figs. 2*C* and 3*C*). Maps of odorant-evoked intraglomerular Ca^{2+} signals should therefore be stable throughout the odor response. Indeed, Ca^{2+} signal maps at different times during odor presentation differed in intensity, but the spatial pattern was always similar (Fig. 3*D*). The correlation between maps evoked by the same odorant in adjacent 1-s time windows ($r = 0.66 \pm 0.16$; $n = 42$) was not significantly different from the correlation between maps evoked by repeated odor applications in the same time window ($P = 0.44$, Wilcoxon rank-sum test).

We next tested whether the pattern of inputs to a glomerulus changes with odor concentration. When odorant concentration was increased from near threshold to near-saturating levels, the response magnitude increased, the response onset became faster, and the time course sometimes acquired a phasic character (Fig. 3*C*). These data are consistent with the concentration dependence of the spiking response of OSNs (40), suggesting that the spiking activity of OSNs is reflected in the calcium signal. However, we observed no recruitment of new Ca^{2+} signal hot spots. Rather, Ca^{2+} signal maps were modulated only in amplitude (Fig. 3*C*). Occasionally, slightly different concentration-response characteristics were observed in different glomerular subregions. For example, in Fig. 3*C*, one region (gray) responded more strongly than the other regions at the lowest, but not the higher concentrations, whereas another region (red) behaved in the opposite manner. However, these effects were small, rare, and not statistically significant. The average correlation between maps evoked by different concentrations ($r = 0.66 \pm 0.17$, $n = 44$; concentrations different by a factor up to 20) was not significantly different from the correlation between maps evoked by repeated application of the same odorant at the same concentration ($P = 0.40$, Wilcoxon rank-sum test). Although most stimuli elicited submaximal responses, we wished to determine whether differences in Ca^{2+} signal maps may be partially obscured by saturation of odorant receptors or the indicator dye. If so, the similarity of maps should decrease when the difference in the overall response intensity (averaged across the entire glomerulus) increases. However, no significant correlation was found between the similarity of response maps and their response intensity ratio ($r^2 = 0.02$; $P > 0.15$; $n = 44$). We therefore conclude that sensory inputs to different regions of a glomerulus show similar odorant sensitivities.

To test whether sensory inputs have different odorant *specificities*, we compared response maps evoked by different odorants in glomeruli for which at least two stimulatory odorants were identified ($n = 16$). Ca^{2+} signal maps evoked by different odorants always seemed similar (Fig. 3*E*), despite substantial differences in the time course and amplitude of responses. The average correlation between maps evoked by different odorants ($r = 0.66 \pm 0.21$) was not significantly different from the correlation between maps evoked by the same odorant ($P = 0.90$, Wilcoxon rank-sum test). Again, the similarity of response maps was not significantly correlated to the ratio of response inten-

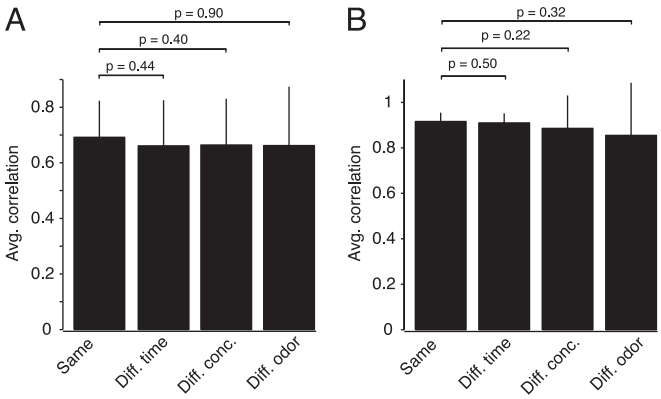

Fig. 4. Statistical analysis of similarity between intraglomerular activity maps. (*A*) Average correlation (±SD) between activity maps evoked by repeated application of the same odorant in the same time window (Same), the same odorant in subsequent 1-s time windows (Diff. time), the same odorant at different concentrations (Diff. conc.), or different odorants (Diff. odor). (*B*) Average correlation between activity maps, after setting ΔF/F values lower than a 30% of the maximum ΔF/F in at least one of the maps in a comparison to 0.

sities ($r^2 = 0.004$; $P > 0.3$). Thus, patterns of sensory input to a glomerulus evoked by different odorants were indistinguishable.

Fig. 4*A* summarizes the results of all correlation analyses. Similar results were obtained when the mean absolute difference was used as a measure of similarity (data not shown). To test whether these results were confounded by noise in nonresponding regions, we also compared responses after thresholding the maps at different levels relative to the maximum ΔF/F (10–50%). This thresholding increased the correlation between response maps, as expected, but maps evoked by different stimuli or at different times were not significantly different from maps evoked by the same stimulus in the same time window (Fig. 4*B*). Hence, patterns of sensory input to a glomerulus measured at different times, and in response to different odorant concentrations and identities, were statistically indiscriminable.

Discussion

Using two-photon Ca^{2+} imaging *in vivo*, we analyzed spatial and temporal patterns of sensory input to individual glomeruli evoked by odorant stimulation. Intraglomerular Ca^{2+} signals were spatially heterogeneous but indiscriminable in their odorant response properties. Thus, at the spatio-temporal resolution of this study, sensory inputs converging onto single glomeruli seem to behave as functional units.

Origin of Presynaptic Ca^{2+} Signals. Several findings indicate that "hot spots" reflect localized Ca^{2+} influx into OSN presynaptic terminals. First, Ca^{2+} signals were negligible in extraglomerular axons (Fig. 1*D*). Second, hot spots were small (≈2 μm). Third, the heterogeneous distribution of Ca^{2+} signals within the neuropil corresponds to that of presynaptic terminals in the glomerulus (34). Finally, the onset of Ca^{2+} signals was often faster than the decay. These properties are consistent with Ca^{2+} signals in other axon terminals, in which presynaptic Ca^{2+} transients are restricted to small volumes around synaptic varicosities, are tightly coupled to action potentials, and have fast onset but slow decay kinetics (41–43).

The small size of most Ca^{2+} signal hot spots implies that the number of underlying OSN terminals is small. Select electron microscopic cross sections show vesicle-containing OSN axon profiles with an average diameter of ≈0.65 μm (Fig. 3*B* in ref. 34). The true diameter of terminal boutons is likely larger, ranging from 0.5 to 2 μm (C. A. Greer, personal communication). Assuming a diameter of 1 μm, the volume of a hot spot would correspond to that of approximately eight boutons. The real number of terminals per hot spot is, however, uncertain because parameters such as bouton size, bouton density, and the spread of calcium inside OSN axons are unknown. Nevertheless, even with a range of between 1 and 100 terminals per hot spot, each hot spot would reflect the activity of only a small fraction of afferent synapses [≈0.001–0.1%; assuming 12,000 OSNs/glomerulus and eight synapses/OSN (2, 3)]. Thus, different hot spots very likely reflect Ca^{2+} signals from a small number of terminals of different OSNs. Comparing Ca^{2+} signals in different hot spots thus serves as a comparison of the odorant response properties of different small subpopulations of inputs converging in the same glomerulus.

Intraglomerular Organization of Ca^{2+} Signals. The patchy distribution of axons and the spatial distribution of Ca^{2+} signals in individual glomerular cross sections is consistent with the intraglomerular segregation of afferent axons and postsynaptic elements (32–35). Our results thus provide functional evidence that synaptic elements within the glomerulus are compartmentalized. In addition, subpopulations of OSNs terminating in circumscribed glomerular subcompartments of a size that is easily resolvable by two-photon microscopy have been defined by histochemical markers (36, 37). We found, however, no evidence for functional subdivisions within a glomerulus on this scale, suggesting that such subcompartments either occur only in a small fraction of glomeruli or that these compartments are functionally equivalent.

Functional Uniformity of OSN Inputs to a Glomerulus. Ca^{2+} signals were measured at a spatial resolution of 1–5 μm. The temporal resolution was likely limited by the kinetics of the Ca^{2+} signals rather than by frame rate and allowed the detection of signal fluctuations ≈200–300 ms in duration (Fig. 2*C*). Differences in response latency, which would not be limited by Ca^{2+} decay kinetics, would have been detectable with higher resolution had they been present. However, we found that patterns of intraglomerular Ca^{2+} signals evoked by odorants of different identity and concentration were indistinguishable. Furthermore, the time course of Ca^{2+} signals, while different for different odorants or concentrations, was similar throughout the glomerulus. These results indicate that convergent sensory inputs show similar odorant specificities, sensitivities, and temporal response properties.

It is possible that odor-dependent differences in Ca^{2+} signals below our resolution limits, e.g., action potential timing differences on a millisecond time scale, were not detected. Moreover, differences between Ca^{2+} signal maps below the limits of our signal-to-noise ratio would not be detectable. If such differences exist, however, they must be small compared to the overall pattern of glomerular input. Our measurements therefore suggest that functional uniformity across OSN afferents and over time is the dominant organizational feature of the sensory input to a glomerulus.

Although convergent OSNs express the same odorant receptor (17–21), the observed functional similarity of glomerular inputs is somewhat surprising. For example, idiotypic OSNs show different odorant sensitivities *in vitro* (26), but patterns of glomerular input did not change significantly as a function of odorant concentration. Also, the scattering of idiotypic OSNs across a large area in the nasal epithelium may be expected to result in different temporal responses *in vivo*. However, we did not observe such differences.

The apparent lack of functional heterogeneity among glomerular inputs may arise from several factors. First, the sensitivity of idiotypic OSNs *in vivo* may be more similar than in dissociated primary culture (26). Second, convergent OSNs are mainly

dispersed along the anterior–posterior axis of the olfactory epithelium (44), where differences in odorant access seem to be relatively small (23, 44). Moreover, the functional similarity of inputs to a glomerulus could be enhanced by multiple mechanisms acting at different sites along OSN axons. Ephaptic coupling of axons in the same olfactory nerve fascicle (45), gap junctions (46, 47), and intraglomerular increases in extracellular K^+ concentration (48, 49) could distribute depolarization across convergent axons. Finally, Ca^{2+} signaling in axon terminals may be modulated by paracrine feedback mechanisms within the glomerulus (29–31). Activity of axon terminals, as monitored by Ca^{2+} imaging, therefore reflects modulated OSN activity at the site of input to the glomerular circuitry, which may be more similar than the patterns of OSN activation in the epithelium.

The Glomerulus as a Functional Unit. Understanding how patterns of neural activity encode information requires the identification of the basic units of which these patterns are composed. Often, the units are individual neurons. The OB glomerulus, in contrast, contains the processes of thousands of neurons. Nevertheless, it has been proposed to function as a unit in odor coding, first because of its circumscribed functional architecture (4, 7, 8), and later based on its innervation by idiotypic OSNs (17–20). This hypothesis is a precondition in most models of combinatorial olfactory coding. Our results support the view of glomeruli as functional units and, thus, validate current models of olfactory coding. Moreover, they suggest that the primary function of the high convergence from OSNs onto mitral/tufted cells (1,000:1) (3) is to improve the signal-to-noise ratio of odor-encoding channels during transmission from OSNs to mitral cells, as opposed to integrating odor information across a functionally diverse array of inputs (12, 50).

It is currently unknown whether the postsynaptic elements of the glomerular circuitry are also functionally similar. Mitral cell apical dendrites are coupled by gap junctions and excitatory glutamatergic mechanisms. These connections amplify afferent input to mitral cells connected to the same glomerulus and synchronize their activity (51–55), suggesting that the glomerular organization may promote the uniform activation of both OSNs and mitral cells. A similar functional organization may exist in glomeruli of *Drosophila* (14, 56). However, individual mitral cells' response properties are also shaped by interneurons providing intra- and interglomerular inhibitory input (57–59), some of which extends far beyond the glomerulus. Network interactions may thus diversify the response properties of mitral cells connected to the same glomerulus, even though their primary afferent input is nearly identical. It will be interesting to examine how sensory inputs channeled through odor-specific sets of glomeruli interact in the OB.

We thank L. Cohen, T. Margrie, N. Urban, and H. Spors for advice, experimental support, and comments on the manuscript. This work was supported by the Max Planck Society.

1. Mombaerts, P. (1999) *Science* **286,** 707–711.
2. Hálasz, N. & Greer, C. A. (1993) *J. Comp. Neurol.* **337,** 307–316.
3. Shepherd, G. M. & Greer, C. A. (1998) in *The Synaptic Organization of the Brain*, ed. Shepherd, G. M. (Oxford Univ. Press, New York), pp. 159–203.
4. Le Gros Clark, W. (1957) *Proc. R. Soc. London Ser. B* **146,** 299–319.
5. Kauer, J. S. & Cinelli, A. R. (1993) *Microsc. Res. Tech.* **24,** 157–167.
6. Hildebrand, J. G. & Shepherd, G. M. (1997) *Annu. Rev. Neurosci.* **20,** 595–631.
7. Shepherd, G. M. (1994) *Neuron* **13,** 771–790.
8. Lancet, D., Greer, C. A., Kauer, J. S. & Shepherd, G. M. (1982) *Proc. Natl. Acad. Sci. USA* **79,** 670–674.
9. Stewart, W. B., Kauer, J. S. & Shepherd, G. M. (1979) *J. Comp. Neurol.* **185,** 715–734.
10. Friedrich, R. W. & Korsching, S. I. (1997) *Neuron* **18,** 737–752.
11. Rubin, B. D. & Katz, L. C. (1999) *Neuron* **23,** 499–511.
12. Wachowiak, M. & Cohen, L. B. (2001) *Neuron* **32,** 723–735.
13. Fried, H. U., Fuss, S. H. & Korsching, S. I. (2002) *Proc. Natl. Acad. Sci. USA* **99,** 3222–3227.
14. Wang, J. W., Wong, A. M., Flores, J., Vosshall, L. B. & Axel, R. (2003) *Cell* **112,** 271–282.
15. Schoppa, N. E. & Urban, N. N. (2003) *Trends Neurosci.* **26,** 501–506.
16. Friedrich, R. W. & Stopfer, M. (2001) *Curr. Opin. Neurobiol.* **11,** 468–474.
17. Ressler, K. J., Sullivan, S. L. & Buck, L. B. (1994) *Cell* **79,** 1245–1255.
18. Vassar, R., Chao, S. K., Sitcheran, R., Nunez, J. M., Vosshall, L. B. & Axel, R. (1994) *Cell* **79,** 981–991.
19. Mombaerts, P., Wang, F., Dulac, C., Chao, S. K., Nemes, A., Mendelsohn, M., Edmondson, J. & Axel, R. (1996) *Cell* **87,** 675–686.
20. Treloar, H. B., Feinstein, P., Mombaerts, P. & Greer, C. A. (2002) *J. Neurosci.* **22,** 2469–2477.
21. Malnic, B., Hirono, J., Sato, T. & Buck, L. B. (1999) *Cell* **96,** 713–723.
22. Ressler, K. J., Sullivan, S. L. & Buck, L. B. (1993) *Cell* **73,** 597–609.
23. Ezeh, P. I., Davis, L. M. & Scott, J. W. (1995) *J. Neurophysiol.* **73,** 2207–2220.
24. Kent, P. F., Mozell, M. M., Murphy, S. J. & Hornung, D. E. (1996) *J. Neurosci.* **16,** 345–353.
25. Mozell, M. M., Sheehe, P. R., Hornung, D. E., Kent, P. F., Youngentob, S. L. & Murphy, S. J. (1987) *J. Gen. Physiol.* **90,** 625–650.
26. Bozza, T., Feinstein, P., Zheng, C. & Mombaerts, P. (2002) *J. Neurosci.* **22,** 3033–3043.
27. Wetzel, C. H., Spehr, M. & Hatt, H. (2001) *Eur. J. Neurosci.* **14,** 1056–1064.
28. Kawai, F., Kurahashi, T. & Kaneko, A. (1999) *Nat. Neurosci.* **2,** 133–138.
29. Aroniadou-Anderjaska, V., Zhou, F. M., Priest, C. A., Ennis, M. & Shipley, M. T. (2000) *J. Neurophysiol.* **84,** 1194–1203.
30. Wachowiak, M. & Cohen, L. B. (1999) *J. Neurosci.* **19,** 8808–8817.
31. Ennis, M., Zhou, F. M., Ciombor, K. J., Aroniadou-Anderjaska, V., Hayar, A., Borrelli, E., Zimmer, L. A., Margolis, F. & Shipley, M. T. (2001) *J. Neurophysiol.* **86,** 2986–2997.
32. Kosaka, K., Toida, K., Margolis, F. L. & Kosaka, T. (1997) *Neuroscience* **76,** 775–786.
33. Chao, T. I., Kasa, P. & Wolff, J. R. (1997) *J. Comp. Neurol.* **388,** 191–210.
34. Kasowski, H. J., Kim, H. & Greer, C. A. (1999) *J. Comp. Neurol.* **407,** 261–274.
35. Potter, S., Zheng, C., Koos, D. S., Feinstein, P., Fraser, S. E. & Mombaerts, P. (2001) *J. Neurosci.* **21,** 9713–9723.
36. Treloar, H., Walters, E., Margolis, F. & Key, B. (1996) *J. Comp. Neurol.* **367,** 550–562.
37. Royal, S. J. & Key, B. (1999) *J. Neurosci.* **19,** 9856–9964.
38. Kauer, J. S. & Moulton, D. G. (1974) *J. Physiol. (London)* **243,** 717–737.
39. Sheppard, C. J. R. & Gu, M. (1990) *Optik* **86,** 104–106.
40. Duchamp-Viret, P., Chaput, M. A. & Duchamp, A. (1999) *Science* **284,** 2171–2174.
41. Cox, C. L., Denk, W., Tank, D. W. & Svoboda, K. (2000) *Proc. Natl. Acad. Sci. USA* **97,** 9724–9728.
42. Regehr, W. G. & Atluri, P. P. (1995) *Biophys. J.* **68,** 2156–2170.
43. Wu, L. G. & Saggau, P. (1994) *J. Neurosci.* **14,** 645–654.
44. Levai, O., Breer, H. & Strotmann, J. (2003) *J. Comp. Neurol.* **458,** 209–220.
45. Bokil, H., Laaris, N., Blinder, K., Ennis, M. & Keller, A. (2001) *J. Neurosci.* **21,** RC173.
46. Zhang, C. & Restrepo, D. (2002) *Brain Res.* **929,** 37–47.
47. Schwartz Levey, M., Cinelli, A. R. & Kauer, J. S. (1992) *Neurosci. Lett.* **140,** 265–269.
48. Jahr, C. E. & Nicoll, R. A. (1981) *J. Physiol. (London)* **318,** 375–384.
49. Friedrich, R. W. & Korsching, S. I. (1998) *J. Neurosci.* **18,** 9977–9988.
50. Cleland, T. A. & Linster, C. (1999) *Neural Comput.* **11,** 1673–1690.
51. Isaacson, J. S. (1999) *Neuron* **23,** 377–384.
52. Schoppa, N. E. & Westbrook, G. L. (2001) *Neuron* **31,** 639–651.
53. Schoppa, N. E. & Westbrook, G. L. (2002) *Nat. Neurosci.* **5,** 1194–1202.
54. Urban, N. N. & Sakmann, B. (2002) *J. Physiol. (London)* **542,** 355–367.
55. Aroniadou-Anderjaska, V., Ennis, M. & Shipley, M. T. (1999) *J. Neurophysiol.* **82,** 489–494.
56. Ng, M., Roorda, R. D., Lima, S. Q., Zemelman, B. V., Morcillo, P. & Miesenböck, G. (2002) *Neuron* **36,** 463–474.
57. Aungst, J. L., Heyward, P. M., Puche, A. C., Karnup, S. V., Hayar, A., Szabo, G. & Shipley, M. T. (2003) *Nature* **426,** 623–629.
58. Shipley, M. T. & Ennis, M. (1996) *J. Neurobiol.* **30,** 123–176.
59. Yokoi, M., Mori, K. & Nakanishi, S. (1995) *Proc. Natl. Acad. Sci. USA* **92,** 3371–3375.